

# Spin-qubit noise spectroscopy from randomized benchmarking by supervised learning

Chengxian Zhang<sup>1</sup> and Xin Wang<sup>1,\*</sup>

<sup>1</sup>*Department of Physics, City University of Hong Kong,  
Tat Chee Avenue, Kowloon, Hong Kong SAR, China,  
and City University of Hong Kong Shenzhen Research Institute, Shenzhen, Guangdong 518057, China*  
(Dated: May 3, 2022)

We demonstrate a method to obtain the spectra of  $1/f$  noises in spin-qubit devices from randomized benchmarking, assisted by supervised learning. The noise exponent, which indicates the correlation within the noise, is determined by training a double-layer neural network with the ratio between the randomized benchmarking results of pulse sequences that correct noise and not. After the training is completed, the neural network is able to predict the exponent within an absolute error of about 0.5, comparable with existing methods. The noise amplitude is then evaluated by training another neural network with the decaying fidelity of randomized benchmarking results from the uncorrected sequences. The relative error for the prediction of the noise amplitude is as low as 5% provided that the noise exponent is known. Our results suggest that the neural network is capable of predicting noise spectra from randomized benchmarking, which can be an alternative method to measure noise spectra in spin-qubit devices.

## I. INTRODUCTION

Noises pose a major challenge to the physical realization of quantum computing. In quantum-dot spin qubits, decoherence is mainly caused by two sources of noises: nuclear noise and charge noise [1]. The nuclear noise (or Overhauser noise) arises from, for example, the hyperfine coupling between the spin of the quantum-dot electron and the nuclear spins surrounding it [2–6]. On the other hand, the charge noise is caused by unintentionally deposited impurities in the fabrication process of the samples, which an electron can hop on and off randomly [7–9]. To combat these noises, dynamically corrected gates (DCGs) [10–16] have been developed for various realizations of spin qubits, some of which have been experimentally demonstrated [17]. Nevertheless, DCGs are mostly developed under the static noise approximation, i.e. the noises are assumed to be slowly varying as compared to the typical gate operation time. Therefore, the effectiveness of reducing noise for the DCGs depends critically on the correlation within the noise or, in the context of  $1/f$  noise (with frequency spectrum  $1/\omega^\alpha$ ) [18], the “exponent”  $\alpha$  [19, 20]. When  $\alpha$  is large, the noise is concentrated in low frequencies and DCGs are most effective. On the contrary, when  $\alpha$  is small, the noise is white-like and DCGs would not offer improvements on the control quality. This suggests that the characterization of noises and, in particular, the interplay between noises and gates is key to successful implementation of quantum computing [21, 22] in quantum-dot spin systems.

Various methods have been used to measure the noise spectra using, for example, optical techniques [23–25]. The exponent of noise can alternatively be obtained through a scaling of the qubit’s response to different orders of dynamical decoupling sequences [26, 27]. Specifi-

cally, the exponent for nuclear noise in a quantum-dot device has been estimated to be  $2.5 \sim 2.6$  [26, 28], while that for charge noise is around  $0.7 \sim 0.8$  [1, 27]. On the other hand, Randomized Benchmarking (RB) has been a tool ubiquitously used to understand the interplay between noises and gates. In numerical simulations of RB, a sequence of gates, randomly drawn from the Clifford group, evolves under certain type of noises [29]. Exponential fitting of the result averaged over many runs gives the average error per gate. These studies have been useful to understand the effectiveness of DCGs undergoing  $1/f$  noise with different exponents [30, 31]. For example, it has been found that DCGs would be effective in reducing noise in singlet-triplet qubits when the  $1/f$  noise exponent is greater than 1 [20], while the threshold for exchange-only qubits is about 1.5 [32]. Nevertheless, the reverse problem, i.e. obtaining the noise spectra from RB results has been difficult.

The development of machine learning [33, 34] and especially supervised learning [35] has provided a viable way to solve the problem. Machine learning is a set of techniques allowing data analysis or optimization in a way much more efficient than many enumerative methods previously known [36, 37]. These techniques have been recently applied to various fields in physics with numerous success [38–46]. In supervised learning, a neural network gets trained using a large amount of data (including inputs and outputs). During the training process, the neurons adjust their parameters to match the input-output correspondence of the training set. Once the network is properly trained, the network is able to make predictions using inputs that are not in the training set. Using this feature, we have explored the possibility of constructing DCGs using supervised learning [47]. It has been demonstrated that the trained neural network is capable of producing the composite pulse sequences that are as robust as the sequences known in the literature [13, 14]. The trained network also enables interchanging the inputs and outputs, which allows us

---

\*Electronic address: [x.wang@cityu.edu.hk](mailto:x.wang@cityu.edu.hk)

to estimate the noise spectra from RB results. In this paper, we demonstrate a method to measure the noise spectrum from RB employing supervised learning. The key to measure the noise spectrum is to determine the two parameters, namely, the noise exponent  $\alpha$  and the noise amplitude  $A$ . We first train the neural network to predict the noise exponent  $\alpha$  by feeding the ratios of the fidelities between the corrected and uncorrected sequences obtained from RB. This idea arises from the fact that the noise exponent  $\alpha$  is key to the efficacy of DCGs [19, 20, 32]. We found that a properly trained neural network is able to predict  $\alpha$  within an error of about  $\pm 0.5$ . On the other hand, there is a positive correlation between the noise amplitude  $A$  and the decaying fidelity provided that the exponent  $\alpha$  is fixed. Once  $\alpha$  is known, the noise amplitude  $A$  can be determined from how fast the fidelity decays for RB results of uncorrected sequences. We are able to predict  $A$  with a relative error of  $\sim 5\%$ .

This paper is organized as follows. In Sec. II, we present the model and methods used in this work. Results are presented and explained in Sec. III. We conclude in Sec. IV.

## II. MODEL AND METHODS

We consider noises of  $1/f$  type. Namely, their power spectral densities have the form

$$S(\omega) = A/(\omega t_0)^\alpha, \quad (1)$$

where  $A$  denotes the noise amplitude, the exponent  $\alpha$  indicates the correlation within the noise, and  $t_0$  is an arbitrary time unit. For small  $\alpha$ , the noise is close to white noise; when  $\alpha$  is large, the noise is concentrated in low frequencies. Therefore, the key of noise spectroscopy is the determination of the two parameters,  $A$  and  $\alpha$ . Traditionally, one generates  $1/f$  noises by summing random telegraph signals [18, 19]. Nevertheless, we have found that this method can only reliably generate noises with exponent  $1/2 \lesssim \alpha \lesssim 3/2$ . In this work, we use an alternative method based on the inverse Fourier transform of noises in the frequency domain, capable to extend the range of the noise exponent to  $0 \leq \alpha \leq 3$  [20]. Fig. 1 shows an example of  $1/f$  noise with  $\alpha = 1.5$ . Note that the frequency has a dimension of the reciprocal of time (equivalent to energy if  $\hbar = 1$ ), therefore it is multiplied by an arbitrary time unit  $t_0$  to make it dimensionless. Both the power spectral density  $S(\omega)$  and the noise amplitude have a dimension of energy (the reciprocal of time if  $\hbar = 1$ ), therefore in later discussions they are also sometimes multiplied by  $t_0$  when dimensionless quantities are desired. Fig. 1(a) depicts the noise as a function of time,  $\xi(t)$ . Fig. 1(b) shows the corresponding dimensionless power spectral density,  $S(\omega)t_0$ , which is close to a straight line under the log scale.

A workhorse to understand the performance of quantum gates subject to time-dependent noises is RB which

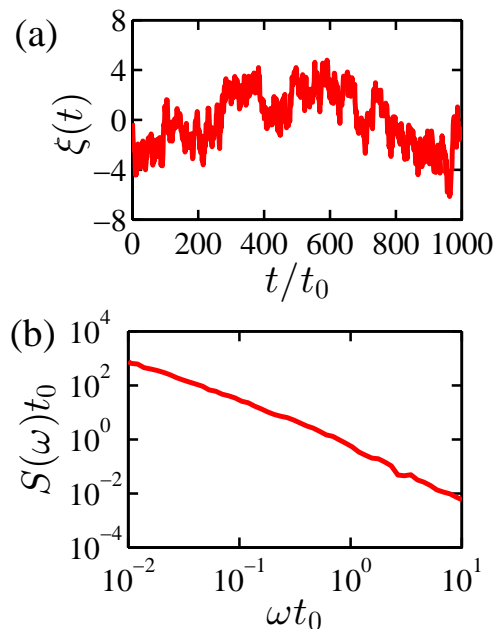


FIG. 1: An example of the  $1/f$  noise used in the simulation. (a) Noise as a function of time. (b) The power spectral density corresponding to the noise shown in (a).  $S(\omega) = A/(\omega t_0)^{1.5}$ . The noise amplitude  $A$  has been scaled so that  $S(\omega = 1/t_0) \approx 1/t_0$ , and  $t_0$  is an arbitrary time unit.

can be simulated on a computer. In simulated (single-qubit) RB, sequences of quantum gates randomly drawn from the 24 single-qubit Clifford gates are executed in presence of noises. Under the assumption that the gate errors are uncorrelated, the fidelity  $F$  decays in an exponential form

$$F = \frac{1}{2} (1 + e^{-\gamma n}), \quad (2)$$

where  $n$  is the number of gates and  $\gamma$  is a parameter closely related to the average error per gate. Essentially, RB takes noises and gates as inputs and the decaying fidelities as outputs. The left column of Fig. 2 [panels (a), (c) and (e)] shows typical results of RB using gates for a singlet-triplet qubit as explained in [19]. The black lines are for “uncorrected” quantum gates, i.e. gates that are not immune to noises. The red/gray lines are for “corrected” gates, which refer to the SUPCODE sequences [13, 14] that are resilient to both nuclear and charge noises. For simplicity, in this work we consider the case that the nuclear and charge noises have the same spectrum, and we shall generically refer to them as “noises”.

For noises with a given spectra and a set of well-defined gates, it is straightforward to run RB simulations and obtain the average error per gate by exponential fitting. Nevertheless, the inverse problem is complicated for two reasons. Firstly, RB is a statistic process during which certain information is lost or suppressed, so it would be hard to recover the noise spectra from just the averaged

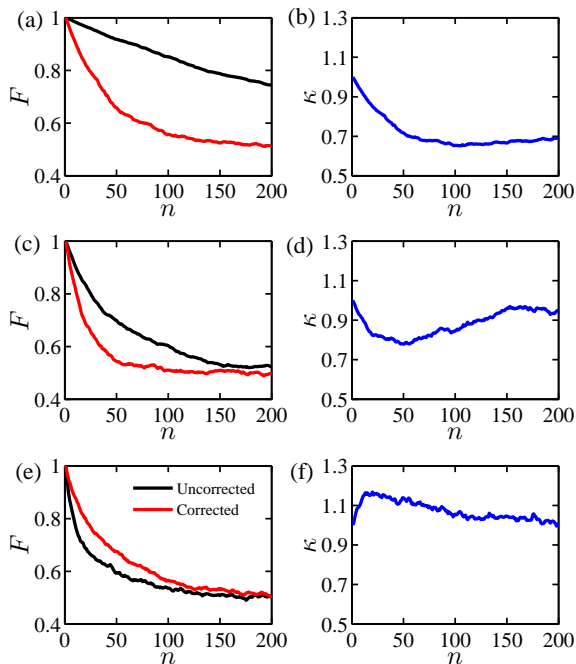


FIG. 2: Randomized benchmarking results of single-qubit Clifford gates subject to  $1/f$  noise with different exponents. (a), (c), (e): The fidelities for uncorrected and corrected gates are shown as black and red/gray lines respectively. (b), (d), (f): The ratios between the corrected and uncorrected sequences corresponds to the results shown on the left. The noise exponents are: (a), (b)  $\alpha = 0$ ; (c), (d)  $\alpha = 1$ ; (e), (f)  $\alpha = 1.5$ . The noise amplitude is fixed by  $At_0 = 10^{-3}$ .

fidelity. Secondly, the noise spectrum contains two key parameters, the noise amplitude  $A$  and exponent  $\alpha$ , both of which contribute to gate errors at the same time and are hard to distinguish. In this work, we shall use the neural network and supervised learning, along with our existing understanding of the interplay between quantum gates and noises, to overcome these difficulties. We shall show that upon judicious training of two neural networks, we will be able to determine the noise amplitude  $A$  to a precision of about 5% (relative error) and the exponent  $\alpha$  to about  $\pm 0.5$  (absolute error) from given inputs of RB data.

Supervised learning [34, 35] is a branch of machine learning which uses a large amount of data to train a neural network. During the training process, the network “learns” from a set of data (“training set”) with known inputs and outputs. Essentially, the parameters governing the network (such as weights and biases) are optimized iteratively such that the outputs of network fit better and better to the known output from the training set. Once the network is properly trained (i.e. the outputs from the network fit known ones to the desired precision), it becomes capable to predict unknown outputs from given inputs. A detailed description of supervised learning and its application in generating composite pulse

sequences to control spin qubits can be found in [47].

Supervised learning provides a viable method to interchange the inputs and outputs of the RB process. Namely, one may train the neural network with the averaged fidelities (outputs from RB) as inputs and the parameters of noise spectra (inputs to RB) as outputs, and the network shall be able to predict the noise spectrum from a known RB result. Nevertheless, since a noise spectrum contain two parameters, the amplitude  $A$  and exponent  $\alpha$ , and they both contribute to the RB results, we must find a way to distinguish the two. On one hand, there is a positive correlation between the noise amplitude  $A$  and the decaying fidelity provided that the exponent  $\alpha$  is fixed. A large  $A$  implies higher noise level, which leads to faster decay of the gate fidelity of the RB results. On the other hand, the noise exponent  $\alpha$  is deeply involved in the efficacy of the noise-correcting composite pulse sequences. Since these sequences are developed with the static noise approximation, they should work for  $1/f^\alpha$  noises with larger  $\alpha$  but not otherwise. This observation has been confirmed in our previous works on SUPCODE [19, 20, 48]. For small  $\alpha$  ( $\alpha \lesssim \alpha_c$  where  $\alpha_c$  is a critical value at which non-correcting sequences and DCGs perform comparably under noise [20]), the noise is white-like, the corrected sequences perform worse than the uncorrected ones. For large  $\alpha$  ( $\alpha \gtrsim \alpha_c$ ), the noise concentrates more at low frequencies and the corrected sequences outperform the uncorrected ones. For SUPCODE and the singlet-triplet qubit, the critical value  $\alpha_c$  is found to be around 1 [20]. This observation can be quantified by the ratio between the fidelity of the two set of states, defined by the fidelity of the corrected gate sequence divided by that of the uncorrected one, and we denote it by  $\kappa$ . The right column of Fig. 2 shows  $\kappa$  corresponding to its counterparts in the left column. For Fig. 2(b) ( $\alpha = 0$ ),  $\kappa$  is smaller than 1 and saturate to a value around 0.7. For Fig. 2(d) ( $\alpha = 1$ ),  $\kappa$  fluctuates around 1. For Fig. 2(f) ( $\alpha = 1.5$ ),  $\kappa$  remains greater than 1. Because the value of  $\kappa$  is related to  $\alpha$ , one may use  $\kappa$  as inputs to the neural network and  $\alpha$  as the output, thereby determining  $\alpha$ .

Summarizing the understandings above, we use a two-step strategy to obtain the noise spectra. We first determine  $\alpha$  by training a neural network with the ratio between the RB results of the corrected and uncorrected sequences as input, and  $\alpha$  as the output. Once  $\alpha$  is determined, we train another neural network with the RB results from either the corrected or uncorrected sequences (in this work the uncorrected ones are used) as inputs and  $A$  as the output, with which  $A$  is determined.

### III. RESULTS

The neural network used in our work has two hidden layers with  $N_n$  neurons each. Fig. 3 schematically shows the structure. For the convenience of later discussions, the default parameters of the neural network are provided

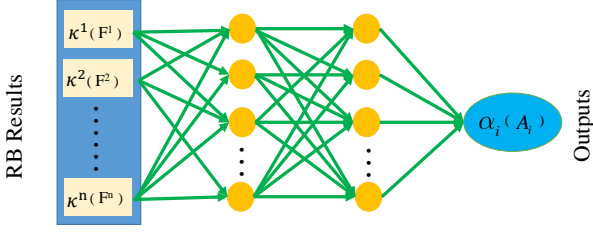


FIG. 3: Schematics of the neural network used in this work. The inputs are given by RB results:  $\kappa$  (corresponding to output of  $\alpha$ ) and  $F$  (corresponding to  $A$ ).  $\kappa$  and  $F$  are discretized into  $\kappa^i$  and  $F^i$  where  $i = 1, \dots, N$  and  $N = 200$ . The neural network contains two hidden layers with  $N_n$  neurons each.

in Table I. One may also refer to the Appendix of [47] for details on the procedure of supervised learning.

In determining  $\alpha$ , the inputs are RB ratios  $\kappa$  between the corrected and uncorrected sequences as functions of the number of gates, which are read to the network as vectors  $\kappa^i$  ( $i = 1, 2, \dots, N$ ) where  $N$  is the number of gates in a sequence used in the simulation. Similarly, in determining  $A$  the inputs are RB results  $F^i$  of the uncorrected sequences assuming that  $\alpha$  is already known. In order to ensure convergence, each data point in the training set is an average of 200 RB simulation results with different gate sequences undergoing different noise realizations for a given noise spectra. For determining  $\alpha$ , the training data points are obtained for different noise spectra with amplitude  $\tilde{A}$  and  $\tilde{\alpha}$  as follows: 50 points of different  $\tilde{\alpha}$  are chosen uniformly on  $\tilde{\alpha} \in (0, 3)$ , and 25 points of different  $\tilde{A}$  are chosen such that  $\log(\tilde{A}t_0)$  distribute uniformly on  $\log(\tilde{A}t_0) \in (-7, -4)$  [20, 32]. For each specific  $\tilde{A}$  and  $\tilde{\alpha}$ , 8 data points (each of which is an average of 200 RB simulations) are generated. Therefore the training data set has  $50 \times 25 \times 8 = 10000$  entries in total. These data are used to train a neural network with training parameters including learning rate  $\eta$ , bin size  $b$ , and number of epochs  $N_e$ . (One may refer to [47] for a detailed explanation of the parameters) The default values of these parameters are provided in Table I but when we use different values they are going to be specified.

For determining  $A$ ,  $\alpha$  is already known (and we have taken  $\alpha = 1.5$  as a representative point). The training data points are therefore obtained for noise with different amplitude  $\tilde{A}$ , chosen such that there are 400 points of  $\log(\tilde{A}t_0)$  distributing uniformly on  $\log(\tilde{A}t_0) \in (-8, -2)$ . For each  $\tilde{A}$ , we generate 25 data points (each of which is an average of 200 RB simulations). The training data set for determining  $A$  therefore has  $400 \times 25 = 10000$  entries in total. These data are used to train a separate neural network in order to determine  $A$ , but the structure of the network is similar to that used to determine  $\alpha$ .

In order to quantify the accuracy of  $\alpha$  predicted by the neural network, we define the average error  $\Delta =$

TABLE I: Default parameters of the neural network.

Number of layers	2
Number of neurons in each layer $N_n$	50
Size of the training data set $N_{\text{tr}}$	5000
Size of a data bin $b$	10
Number of training epochs $N_e$	1000
Activation function $f(z)$	$1/(1 + e^{-z})$
Learning rate $\eta$	0.005

$\frac{1}{n} \sum_{i=1}^n |\alpha - \alpha_i|$  where  $\alpha$  is the known noise exponent and  $\alpha_i$  the corresponding predicted one, and  $n$  is the number of data points available for testing. In Fig. 4, we plot  $\Delta$  as functions of the number of epochs for different training parameters, including the learning rate  $\eta$ , bin size  $b$  and number of neurons in each layer  $N_n$ . The left column [panels (a), (c) and (e)] shows results with the size of training set  $N_{\text{tr}} = 5000$ , while the right column [panels (b), (d) and (f)] shows results for  $N_{\text{tr}} = 10000$ . It is clear that in all cases, results with a larger training set are better than ones with a smaller training set, as the errors of predicted  $\alpha$  converge to a lower value in the right column as compared to the left one.

Fig. 4(a) and (b) show results with different training rates,  $\eta$ . For small  $\eta$ , the error goes down with more epochs smoothly but slowly, while for larger  $\eta$ , the error goes down more steeply but is unstable, i.e. more oscillations can be seen. For  $\eta = 0.001$ , the average error reduce to 0.6 for the case with  $N_{\text{tr}} = 10000$ , significantly larger than the other cases. Since the average errors for both  $\eta = 0.005$  and  $\eta = 0.01$  converge to 0.5 but that for  $\eta = 0.01$  is more unstable, we consider  $\eta = 0.005$  an appropriate value for the learning rate. Fig. 4(c) and (d) show results with different bin sizes. When the bin size is large (e.g.  $b \geq 20$ ), the error goes down slower than the case with a smaller bin size. However, when the training data is noisy, a bin size which is too small could potentially lead to overfitting on the noisy details of the data. Since the results for  $b = 10$  do not show signs of overfitting, we consider  $b = 10$  appropriate for this training. Fig. 4(e) and (f) show results with different number of neurons in each hidden layer. While increasing the number of neurons may improve the ability of the network to fit the training data, we see that for the case with  $N_{\text{tr}} = 10000$ , the difference is not large. For the case with  $N_{\text{tr}} = 5000$ , result for  $N_n = 10$  is notably worse than the other two cases, while the result for  $N_n = 50$  is the best with the lowest error. We therefore take  $N_n = 50$  as the default parameter of the neural network. Overall we have shown that with proper training, the neural network can predict  $\alpha$  with an accuracy of about 0.5 (absolute error). While the accuracy may not be as high as expected, we should note that it is already on par with existing methods based on dynamical decoupling [26, 27].

Next we proceed to show the results of predicting the noise amplitude  $A$  in Fig. 5. Since the value of  $A$

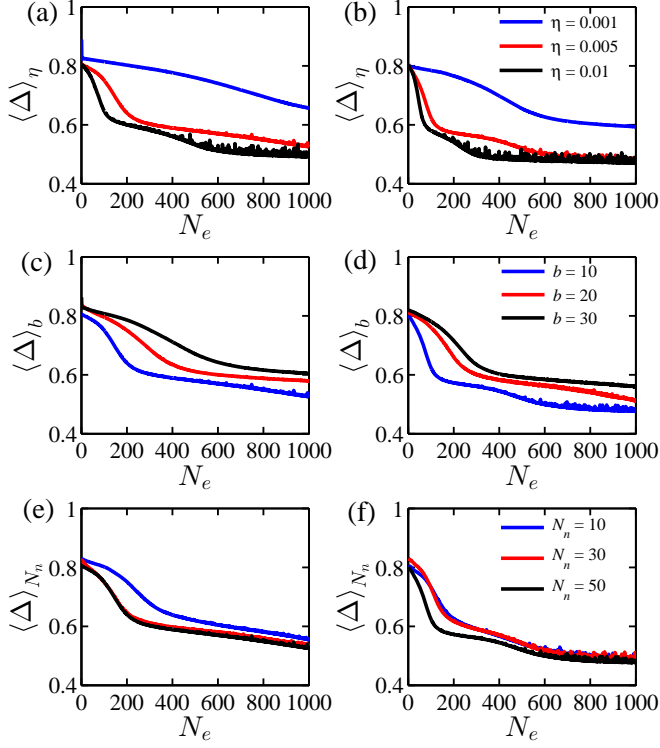


FIG. 4: The averaged error  $\Delta$  for the noise exponent  $\alpha$  as functions of the number of epochs. The left column [panels (a), (c) and (e)] corresponds to a training set with 5000 entries, while the right column [panels (b), (d) and (f)] corresponds to a training set with 10000 entries. For panels (a) and (b), the blue (upper) line, red (middle) line and black (bottom) line show results with learning rates  $\eta = 0.001, 0.005$  and  $0.01$  respectively, while other parameters are fixed at  $b = 10$  and  $N_n = 50$ . For panels (c) and (d), the blue (bottom) line, red (middle) line and black (upper) line show results with bin size  $b = 10, 20$  and  $30$  respectively, while other parameters are fixed at  $\eta = 0.005$  and  $N_n = 50$ . Lines in panels (e) and (f) show results with  $N_n = 10, 30$  and  $50$  respectively while other parameters are fixed at  $\eta = 0.005$  and  $b = 10$ .

may span several orders of magnitude, and  $A$  is always nonzero, we consider the averaged *relative* error of  $A$ , defined as  $\delta = \frac{1}{n} \sum_{i=1}^n \left| \frac{A - A_i}{A} \right|$  where  $A$  is the known noise amplitude, and  $A_i$  the predicted one. Similar to the previous case of determining  $\alpha$ , we prepare two training data sets, one with  $N_{\text{tr}} = 5000$  (shown as the left column of Fig. 5) and one with  $N_{\text{tr}} = 10000$  (right column of Fig. 5). Qualitatively, the results are similar to Fig. 4. The saturated error is smaller for the network trained by a larger training set. Fig. 5(a) and (b) show results with different learning rates  $\eta$ . Again,  $\eta = 0.001$  is too small and the error is not reduced efficiently. For  $N_{\text{tr}} = 10000$  results (Fig. 5(b)), both lines for  $\eta = 0.005$  and  $\eta = 0.01$  converge to the relative error level around 5%. Fig. 5(c) and (d) show results with different bin sizes  $b$ . While different bin sizes make considerable differences in Fig. 5(c) ( $N_{\text{tr}} = 5000$ ), they all converge to the relative error about

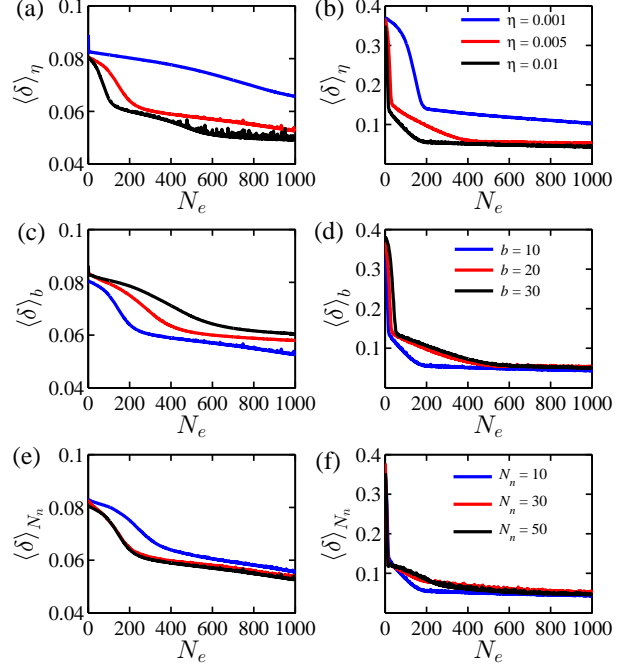


FIG. 5: The (dimensionless) averaged relative error  $\delta$  for the noise amplitude  $At_0$  as functions of the number of epochs. The left column [panels (a), (c) and (e)] corresponds to a training set with 5000 entries, while the right column [panels (b), (d) and (f)] corresponds to a training set with 10000 entries. For panels (a) and (b), the blue (upper) line, red (middle) line and black (bottom) line show results with learning rates  $\eta = 0.001, 0.005$  and  $0.01$  respectively. For panels (c) and (d), the blue (bottom) line, red (middle) line and black (upper) line show results with bin size  $b = 10, 20$  and  $30$  respectively. Lines in panels (e) and (f) show results with  $N_n = 10, 30$  and  $50$ . Except where explicitly noted, the parameters are set at their default values as in Table I.

5% in Fig. 5(d) ( $N_{\text{tr}} = 10000$ ). The behavior is similar in Fig. 5(e) and (f) where results for different number of neurons in each hidden layer are displayed. Again, when the training set has  $N_{\text{tr}} = 10000$  data points, the relative error for all cases converge to around 5%. Overall, we have shown that a properly trained neural network can predict the noise amplitude of a device to an accuracy of about 5%, provided that the noise exponent  $\alpha$  is known.

#### IV. CONCLUSIONS

To conclude, we have shown that judiciously trained neural networks can be used to measure the spectrum of  $1/f$  noise. We determine the noise exponent  $\alpha$  and the amplitude  $A$  through a two-step process. Firstly, we perform RB for DCGs and gates not immune to noise. The ratio between the RB fidelities of the two sets of gates are fed to a double-layer neural network as inputs and the known noise exponents as the outputs for train-

ing. We found that after the neural network is properly trained, it can predict the noise exponent with an absolute error about  $\pm 0.5$ . Then we perform RB with only the uncorrected pulse sequences and use their decaying fidelities as inputs to another neural network, while the noise amplitudes are outputs. We then show that provided the noise exponent is known, the neural network can predict the noise amplitude with a relative error of  $\sim 5\%$ . Overall, we have shown that supervised learning in combination with RB provides an alternative method to measure the noise spectrum in quantum-dot devices. Lastly, we note that the  $1/f$  noise we considered in our

study is a rather simplified case. Evaluating noises with more complicated spectra is in principle possible with RB and machine learning, but would require more complex neural networks as well as more extensive training processes.

This work is supported by the Research Grants Council of the Hong Kong Special Administrative Region, China (No. CityU 21300116, CityU 11303617), the National Natural Science Foundation of China (No. 11604277), and the Guangdong Innovative and Entrepreneurial Research Team Program (No. 2016ZT06D348)

- 
- [1] A. V. Kuhlmann, J. Houel, A. Ludwig, L. Greuter, D. Reuter, A. D. Wieck, M. Poggio, and R. J. Warburton, *Nat. Phys.* **9**, 570 (2013).
  - [2] F. H. Koppens, J. A. Folk, J. M. Elzerman, R. Hanson, L. W. Van Beveren, I. T. Vink, H.-P. Tranitz, W. Wegscheider, L. P. Kouwenhoven, and L. M. Vandersypen, *Science* **309**, 1346 (2005).
  - [3] D. J. Reilly, J. M. Taylor, E. A. Laird, J. R. Petta, C. M. Marcus, M. P. Hanson, and A. C. Gossard, *Phys. Rev. Lett.* **101**, 236803 (2008).
  - [4] L. Cywiński, W. M. Witzel, and S. Das Sarma, *Phys. Rev. B* **79**, 245314 (2009).
  - [5] E. Barnes, L. Cywiński, and S. Das Sarma, *Phys. Rev. Lett.* **109**, 140403 (2012).
  - [6] E. Chekhovich, M. Makhonin, A. Tartakovskii, A. Yacoby, H. Bluhm, K. Nowack, and L. Vandersypen, *Nat. Mater.* **12**, 494 (2013).
  - [7] X. Hu and S. Das Sarma, *Phys. Rev. Lett.* **96**, 100501 (2006).
  - [8] D. Culcer, X. Hu, and S. Das Sarma, *Appl. Phys. Lett.* **95**, 073102 (2009).
  - [9] N. T. T. Nguyen and S. Das Sarma, *Phys. Rev. B* **83**, 235322 (2011).
  - [10] K. Khodjasteh, D. A. Lidar, and L. Viola, *Phys. Rev. Lett.* **104**, 090501 (2010).
  - [11] M. D. Grace, J. M. Dominy, W. M. Witzel, and M. S. Carroll, *Phys. Rev. A* **85**, 052313 (2012).
  - [12] T. Green, H. Uys, and M. J. Biercuk, *Phys. Rev. Lett.* **109**, 020501 (2012).
  - [13] X. Wang, L. S. Bishop, J. P. Kestner, E. Barnes, K. Sun, and S. Das Sarma, *Nat. Commun.* **3**, 997 (2012).
  - [14] J. P. Kestner, X. Wang, L. S. Bishop, E. Barnes, and S. Das Sarma, *Phys. Rev. Lett.* **110**, 140502 (2013).
  - [15] G. T. Hickman, X. Wang, J. P. Kestner, and S. Das Sarma, *Phys. Rev. B* **88**, 161303(R) (2013).
  - [16] F. Setiawan, H.-Y. Hui, J. P. Kestner, X. Wang, and S. D. Sarma, *Phys. Rev. B* **89**, 085314 (2014).
  - [17] X. Rong, J. Geng, Z. Wang, Q. Zhang, C. Ju, F. Shi, C.-K. Duan, and J. Du, *Phys. Rev. Lett.* **112**, 050503 (2014).
  - [18] L. K. Castelano, F. F. Fanchini, and K. Berrada, *Phys. Rev. B* **94**, 235433 (2016).
  - [19] X. Wang, L. S. Bishop, E. Barnes, J. P. Kestner, and S. Das Sarma, *Phys. Rev. A* **89**, 022310 (2014).
  - [20] X.-C. Yang and X. Wang, *Sci. Rep* **6**, 28996 (2016).
  - [21] P. Peddibhotla, F. Xue, H. I. T. Hauge, S. Assali, E. P. A. M. Bakkers, and M. Poggio, *Nat. Phys.* **9**, 631 (2013).
  - [22] J. Hansom, C. H. Schulte, C. Le Gall, C. Matthiesen, E. Clarke, M. Hugues, J. M. Taylor, and M. Atatüre, *Nat. Phys.* **10**, 725 (2014).
  - [23] B. Urbaszek, X. Marie, T. Amand, O. Krebs, P. Voisin, P. Maletinsky, A. Högele, and A. Imamoglu, *Rev. Mod. Phys.* **85**, 79 (2013).
  - [24] P. Glasenapp, N. A. Sinitsyn, L. Yang, D. G. Rickel, D. Roy, A. Greilich, M. Bayer, and S. A. Crooker, *Phys. Rev. Lett.* **113**, 156601 (2014).
  - [25] N. A. Sinitsyn and Y. V. Pershin, *Rep. Prog. Phys.* **79**, 106501 (2016).
  - [26] J. Medford, L. Cywiński, C. Barthel, C. M. Marcus, M. P. Hanson, and A. C. Gossard, *Phys. Rev. Lett.* **108**, 086802 (2012).
  - [27] O. E. Dial, M. D. Shulman, S. P. Harvey, H. Bluhm, V. Umansky, and A. Yacoby, *Phys. Rev. Lett.* **110**, 146804 (2013).
  - [28] M. S. Rudner, F. H. L. Koppens, J. A. Folk, L. M. K. Vandersypen, and L. S. Levitov, *Phys. Rev. B* **84**, 075339 (2011).
  - [29] E. Magesan, J. M. Gambetta, and J. Emerson, *Phys. Rev. A* **85**, 042311 (2012).
  - [30] C. Zhang, R. E. Throckmorton, X.-C. Yang, X. Wang, E. Barnes, and S. Das Sarma, *Phys. Rev. Lett.* **118**, 216802 (2017).
  - [31] R. E. Throckmorton, C. Zhang, X.-C. Yang, X. Wang, E. Barnes, and S. Das Sarma, *Phys. Rev. B* **96**, 195424 (2017).
  - [32] C. Zhang, X.-C. Yang, and X. Wang, *Phys. Rev. A* **94**, 042323 (2016).
  - [33] P. Mehta, M. Bukov, C.-H. Wang, A. G. R. Day, C. Richardson, C. K. Fisher, and D. J. Schwab, *arXiv:1803.08823* (2018).
  - [34] M. Mohri, A. Rostamizadeh, and A. Talwalkar, *Foundations of Machine Learning* (The MIT Press, Cambridge, 2012).
  - [35] M. A. Nielsen, *Neural Networks and Deep Learning* (Determination Press, 2015).
  - [36] M. I. Jordan and T. M. Mitchell, *Science* **349**, 255 (2015).
  - [37] Y. LeCun, Y. Bengio, and G. Hinton, *Nature* **521**, 436 (2015).
  - [38] R. Biswas, L. Blackburn, J. Cao, R. Essick, K. A. Hodge, E. Katsavounidis, K. Kim, Y.-M. Kim, E.-O. Le Bigot, C.-H. Lee, J. J. Oh, S. H. Oh, E. J. Son, Y. Tao, R. Vaulin, and X. Wang, *Phys. Rev. D* **88**, 062003 (2013).

- (2013).
- [39] S. V. Kalinin, B. G. Sumpter, and R. K. Archibald, *Nat. Mater.* **14**, 973 (2015).
  - [40] J. Biamonte, P. Wittek, N. Pancotti, P. Rebentrost, N. Wiebe, and S. Lloyd, *Nature* **549**, 195 (2017).
  - [41] G. Reddy, A. Celani, T. J. Sejnowski, and M. Vergassola, *Proc. Natl. Acad. Sci. U.S.A.* **113**, E4877 (2016).
  - [42] S. S. Schoenholz, E. D. Cubuk, D. M. Sussman, E. Kaxiras, and A. J. Liu, *Nat. Phys.* **12**, 469 (2016).
  - [43] L. Wang, *Phys. Rev. B* **94**, 195105 (2016).
  - [44] E. P. L. van Nieuwenburg, Y.-H. Liu, and S. D. Huber, *Nat. Phys.* **13**, 435 (2017).
  - [45] G. Carleo and M. Troyer, *Science* **355**, 602 (2017).
  - [46] M. Bukov, A. G. R. Day, D. Sels, P. Weinberg, A. Polkovnikov, and P. Mehta, *Phys. Rev. X* **8**, 031086 (2018).
  - [47] X.-C. Yang, M.-H. Yung, and X. Wang, *Phys. Rev. A* **97**, 042324 (2018).
  - [48] X. Wang, F. A. Calderon-Vargas, M. S. Rana, J. P. Kestner, E. Barnes, and S. Das Sarma, *Phys. Rev. B* **90**, 155306 (2014).